JOURNAL OF CATALYSIS **169,** 33–44 (1997)
ARTICLE NO. CA971694

Synthesis and Characterization of High Specific Surface Area Vanadium Carbide; Application to Catalytic Oxidation

Frédéric Meunier,* Pascale Delporte,* Baudouin Heinrich,* Christophe Bouchy,* Claude Crouzet,* Cuong Pham-Huu,* Pierre Panissod,† Jan J. Lerou,‡ Patrick L. Mills,‡ and Marc J. Ledoux*,[1]

*Laboratoire de Chimie des Matériaux Catalytiques, Ecole Européenne de Chimie, Polymères et Matériaux (ECPM), Université Louis Pasteur (ULP), 1 rue Blaise Pascal, 67000, Strasbourg, France; †GEMME, Institut de Physique et Chimie des Matériaux de Strasbourg, 23 rue du Loess, 67037 Strasbourg Cedex, France; and ‡Du Pont Central Research & Development, Experimental Station, Wilmington, Delaware 19880-0304

Received October 29, 1996; revised February 24, 1997; accepted March 14, 1997

A method initially developed for the synthesis of high surface area carbides using volatile metallic precursors was successfully adapted to the preparation of high surface area vanadium carbide using a liquid precursor. The method consists of reacting metallic oxide vapours with activated charcoal to form the corresponding carbide which keeps the shape of the high surface area charcoal (shape memory synthesis). In the present extension of the method, the vanadium oxide V_2O_5 is liquid instead of being gas; V_2O_5 melts and spreads over the carbonaceous frame (1150 $m^2\ g^{-1}$) as soon as it is heated to its melting point. Due to its good wetting properties, V_2O_5 covers the charcoal surface homogeneously. By further thermal treatment, the oxidic layer is reduced and carburized by the carbon, yielding a vanadium carbide which retains a very high dispersion. The composite product, still containing some carbon in its bulk, covered by carbide, exhibits a surface area greater than 200 $m^2\ g^{-1}$. After careful passivation in air the vanadium carbide presents a superficial amorphous layer of 4 to 30 nm. This superficial layer contains oxygen. The pure vanadium carbide is air sensitive at room temperature and slowly reoxidises. This material is then tested as catalyst for the controlled oxidation of butane into maleic anhydride. Under rich mixture butane/oxygen V_8C_7 is stable but not selective yielding large amounts of CO and CO_2; under lean mixture the catalyst is transformed into different vanadium oxycarbides and oxides, one of these oxycarbides being very active and selective when compared to a conventional VPO catalyst.

1. INTRODUCTION

The transition metal carbides, pure or modified by oxygen, have been extensively studied as a new class of catalysts, due to their attractive advantages in terms of activity, selectivity, stability, and resistance to poisoning in hydrocarbon reactions (1–13). These materials also exhibit interesting mechanical hardnesses and high melting points (14–15), that make them more resistant to sintering and attrition than other solids. A major problem related to these materials was the low surface area obtained when they were prepared according to the traditional solid–solid methods (0.1 to 1 $m^2\ g^{-1}$), a serious handicap in catalytic applications. Over the last decade, much work has been done on the synthesis of carbides with high specific surface area (HSS) using several techniques such as temperature-programmed reaction (2, 5–7, 18–20) and reduction-carburization by means of CO, $CO + CO_2$, or $CO + H_2$ (17–20); some authors have obtained very satisfactory results (100–200 $m^2\ g^{-1}$). However, there are two main problems in the synthesis of the HSS transition metal carbides by these different methods: 1. the synthesis is usually long and delicate and requires complex monitoring during the carburization period; 2. whatever the method used, the carbide surface is polluted by polymeric carbon which plugs the pores and covers the active sites. This carbon comes from the decomposition of the reactive mixture (light hydrocarbon, CO, $CO + CO_2$, or $CO + H_2$) and is difficult to remove.

Recently, a new synthetic route was proposed by Ledoux *et al.* (16–17) for the preparation of high surface area silicon carbide for use as a catalytic support which avoids the formation of carbon residues on the surface. It is the solid carbon which is now attacked by an oxide vapour instead of the reverse reaction, where a solid oxide was reacted with a vapour containing carbon atoms. In addition, the formation of CO which can be pumped off is the driving force of the reaction. The authors subsequently adapted this method to the synthesis of high surface area Mo and W carbides (10). This article discusses the synthesis and characterization of the high specific surface area vanadium carbide obtained by a similar route and subsequently its use as a catalyst for butane oxidation into maleic anhydride. The synthesis method is here extended to the use of liquid oxides. The solid materials are characterized by several physical techniques such as powder X-ray diffraction (XRD), measurement of the specific surface area by the BET technique, atomic absorption, scanning electron microscopy (SEM), temperature-programmed reduction (TPR), ^{51}V

[1] To whom all correspondence should be addressed.

0021-9517/97 $25.00

metal solid NMR, and ^{13}C magic angle spinning NMR (MAS-NMR). The microstructure is characterized by high resolution transmission electron microscopy (HRTEM).

2. EXPERIMENTAL

2.1. Synthesis

The vanadium carbide was prepared by reacting a mechanical mixture of V_2O_5 (Strem Chemical, purity >99.95%, granulometry <50 mm) and an activated carbon (Fluka, Puriss) with a high specific surface area (1150 $m^2 g^{-1}$, granulometry 250–425 mm, oxygen content 9.2 wt%). The initial amounts of reactants were of 1 g of charcoal and 1.5 g of V_2O_5. The synthesis was made by heating the mechanical mixture of both reactants in a graphite crucible placed in between induction wires, under dynamic vacuum (60Pa) (10). The pressure in the chamber was measured by a Pirani gauge and the temperature by an infra-red pyrometer. The reaction can be described by the equilibrium

$$\underset{\text{liquid}}{V_2O_5} + x\underset{\text{solid}}{C} \rightleftarrows 2\underset{\text{solid}}{VC} + y\underset{\text{gas}}{CO_z}.$$

The products CO_2 and CO were pumped-off from the furnace as the only gaseous species, thus shifting the reaction equilibrium towards its right-hand side. After synthesis, the material was cooled down rapidly to room temperature, still under dynamic vacuum, and then passivated by slow exposure to air leaking into the reactor. In order to prevent subsequent reaction with air or moisture, the sample was stored in a glove box under a nitrogen atmosphere until further characterization.

2.2. Characterization Techniques

The structural characterization of the samples was done by powder X-ray diffraction (XRD), SEM, high resolution TEM, and NMR analyses. XRD measurements were performed on a Siemens Model D-500 diffractometer using Co $K\alpha_1$ radiation. The average particle size was determined using the conventional Scherrer equation, $d = 0.9\lambda/B\cos\theta$, where d is the particle diameter, λ is the X-ray wavelength, θ is the Bragg angle, and B is the extra peak broadening due to the particle size effect, corrected from the instrumental width.

The morphology was studied by scanning electron microscopy (SEM) using a Jeol Model JMS 840. The samples were generally embedded in a neutral resin, cut, polished, and, after being fixed on the sample holder, covered in situ by a thin layer of gold. Elemental analysis was performed by EDAX. A TOPCON EM002B UHR electron microscope operating at 200 keV for high resolution transmission electron microscopy (HRTEM) was also used. To prevent artifacts due to contamination, no solvents were ever added at any stage and samples were prepared by grinding the catalysts between glass plates and bringing the powder into contact with a holey carbon-coated copper grid. EDX microanalysis was used to provide the complementary data on the elemental composition; the corresponding spectra are not reported. Great care was taken during the HRTEM experiments in order to avoid heating effects of the incident beam. The samples were stable enough to allow a magnification of 590,000x or more.

The ^{51}V solid state nuclear magnetic resonance (NMR) and the ^{13}C MAS-NMR were also used to characterize the vanadium carbide. The ^{51}V solid state NMR analysis was performed on a Brucker Model CXP-100 pulsed spectrometer equipped with a box-car integrator; 500.0 ± 0.1 mg of carbide was introduced into the cell and the spectra were recorded at the temperature of liquid nitrogen (77 K) or helium (4.2 K) to improve the sensitivity. The spectra were obtained using a spin-echo technique by scanning the magnetic field and digitally recording the spin-echo intensity yielded by the box-car integrator versus the applied induction field intensity (21). The apparatus frequency was set at 18 577 kHz and the field was swept between 15.0 and 18.0 kOe to cover the ^{51}V NMR spectrum. The ^{13}C MAS-NMR analysis was performed on a Brucker Model MSL-400. The induction field was of 9.395 T, and the spectra were recorded at room temperature using adamantane as an internal standard. The rotation frequency chosen was above 10 kHz.

The surface areas were measured by the single point BET method using a Carlo Erba Ins. Model Sorpty 1750 (two independent measures for each sample). The sample was outgased for 1 h at 580 K at 5 Pa before analysis which was carried out at 18 kPa and at 77 K with nitrogen (Air Liquide, 99.95%) as adsorbate. Temperature programmed reduction (TPR) was performed under hydrogen flow (10 ml/min), purified by a series of traps containing silicagel and molecular sieves, in a temperature range of 273 to 1073 K, this temperature being increased at a rate of 20 K/min. The water formed by reduction was analyzed by a TCD detector.

The evaluation of the unreacted charcoal present in the sample was made by dissolution of the oxides and/or the carbides in aqua regia.

2.3. Catalytic Tests

A micropilot was specially built for the catalytic test (Fig. 1). Three main problems had to be tackled to realize such a system: (1) the complexity of the gas mixture and the excursion into the explosive range; (2) the high melting point of the product (maleic anhydride Eb = 475 K); (3) the difficulty in the product analysis (light gases, oxygenated molecules mixed to hydrocarbons) in order to obtain a precise mass balance.

The gas mixtures were prepared from six cylinders (Air liquide): pure butane, He/O_2 80/20 and 50/50, pure He, He/CH_4 60/40, and pure nitrogen. An all-metallic tube

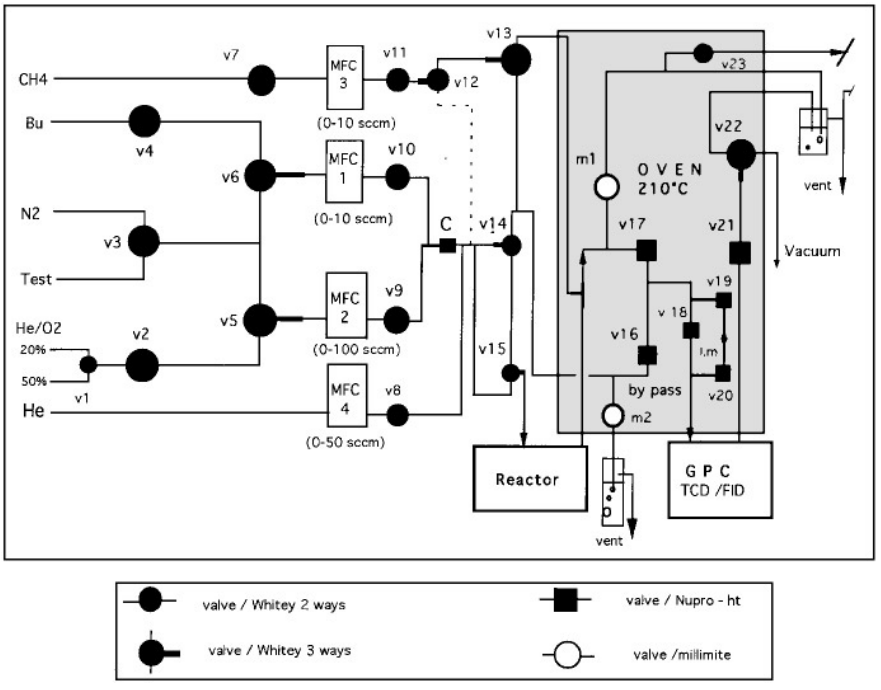

FIG. 1. The micropilot for catalytic tests: butane oxidation.

system, organized with 12 valves (two- and three-way), plus four mass flow controllers, was connected to a fixed-bed reactor in silica-steel (steel tube with the internal wall coated with silica) which could contain up to 3 g of catalyst. The reactor was placed in an oven, with the temperature regulated at ± 0.5 K from room temperature up to 973 K. The gas mixture flow could be varied from 1 to 100 cc/min in all required ratios butane/oxygen/helium.

In order to get rid of the condensation of the maleic anhydride, all pipes and tubing after the reactor were enclosed in an oven heated above 483–493 K. The vent was bubbling in water to transform maleic anhydride into the corresponding acid and consequently avoid the formation of a solid block of anhydride at the outlet.

The on-line gas chromatography was built around a Varian 3300 gas chromatograph (connected to a Compaq PC) equipped with two capillary columns heated from 333 to 383 K during the analyses. The first column, adapted to a TCD detector (He vector gas), Carboplot from Chrompack was used for the separation and analysis of the following products: He, O_2, CO, CH_4, and CO_2. The second column, adapted to a FID detector (H_2 vector gas), DB1 from JNW Scientific was used for the separation and analysis of the following products: all hydrocarbons (CH_4, butane, and butenes here) and oxygenated products (acetone, methacrolein, acrylic acid, crotonaldehyde, and maleic anhydride here). The injection of a known amount of CH_4 into the gas flow after the reactor allowed a very accurate carbon and oxygen mass balance to be reached; two independent loops were used to inject the products into the two columns.

3. RESULTS AND DISCUSSION

3.1. XRD and SEM Analyses

A series of materials was prepared at 1563 K; due to the thermal inertia of the crucible, about 1 h was necessary to reach this temperature. The temperature profile and the pressure variation during this lag time are reported in Fig. 2; charcoal alone and charcoal + V_2O_5 were studied. The low residual pressure when pure charcoal was heated showed that outgassing was not responsible for the significant variation in pressure observed during the synthesis, corresponding mainly to CO formation and release. The synthesis was stopped at regular time intervals. The microscopic structure of the samples was investigated by

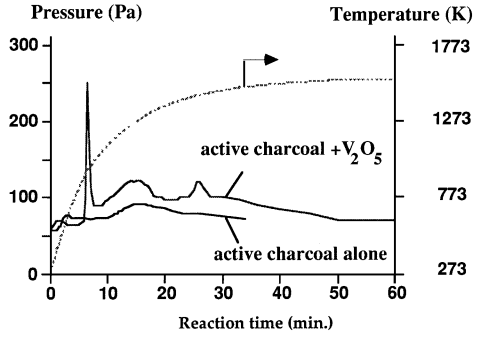

FIG. 2. Evolution of the chamber pressure and the crucible temperature with the reaction time.

TABLE 1

XRD, BET, and Charcoal Consumption versus Time of Reaction (Initial Reactant Masses: 1.000 g of Active Charcoal and 1.514 g of V_2O_5)

Reaction time (min)	6	7.5	21	30	40	60	2×60	4×60	7×60
Temperature (K)	893	993	1393	1473	1526	1548	1563	1563	1563
Sample colour	Brown powder + black particles	Light blue	Dark grey	Grey	Light grey	Light grey	Light grey	Light grey	Light grey
XRD analysis (listed by decreasing intensity)	V_2O_5	VO_2	V_2O_3	V_2O_3 V_8C_7	V_8C_7 V_2O_3 $VO_{0.9}$	V_8C_7 $VO_{0.9}$ V_2O_3 V_2C	V_8C_7 $VO_{0.9}$ V_2C	V_8C_7 V_2C $VO_{0.9}$	V_8C_7
Surface area ($m^2\ g^{-1}$)	447	491	391	359	344	268	234	230	237
Remaining charcoal (wt%)	44	46	46	42	40	39	38	33	28

Note. Atomic ratio (C/V = 5).

XRD; their BET surface area and the remaining unreacted charcoal were measured (Table 1).

Six minutes after the beginning of the heating process, the two reactants charcoal and V_2O_5 were still discernable, both by their different particle sizes and colours. V_2O_5 was superficially brown, but still orange in the bulk and presented the XRD pattern of pure V_2O_5 (Fig. 3a). The brown surface was probably due to the beginning of the reduction which can occur under heating even in a nonreductive atmosphere (22).

The first sharp pressure peak was observed after 7 min and a temperature of 950 ± 10 K which corresponds to the melting point of V_2O_5. V_2O_5 particles had disappeared and only the ex-charcoal particles were remaining, but now coloured light blue instead of black. The XRD showed the presence of VO_2 and an increase in the background noise which generally accompanies a "de-crystallisation" or an amorphisation of the sample (Fig. 3b). A SEM cross section view of a particle is shown in Fig. 4. The bright areas were identified as vanadium species by a line scan analysis detecting the Kα-vanadium ray (not reported). Vanadium had deeply and homogeneously penetrated the pores of the charcoal particles. The remaining large dark areas were assigned to unreacted charcoal. At this low temperature only a liquid impregnation is possible while with MoO_3 the

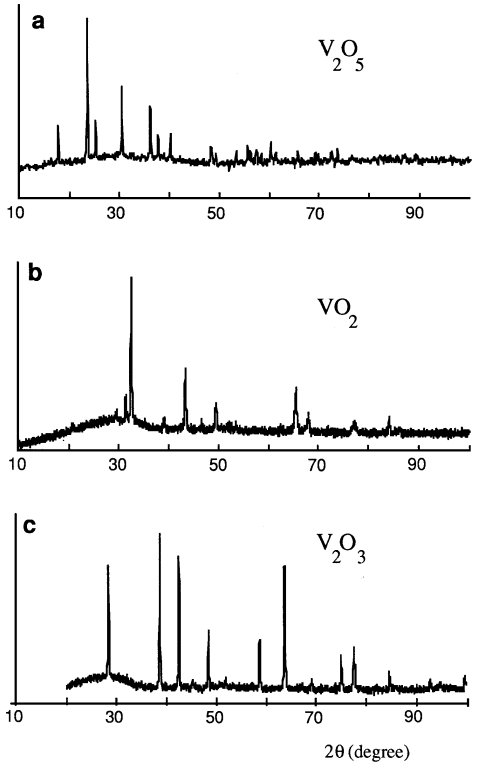

FIG. 3. XRD pattern of the intermediate at: (a) 6 min and 893 K, JCPDS 9-387; (b) 7.5 min and 993 K, JCPDS 33-1440 and 31-1438; (c) 21 min and 1393 K, JCPDS 34-187. Y-scale: intensity (a.u.).

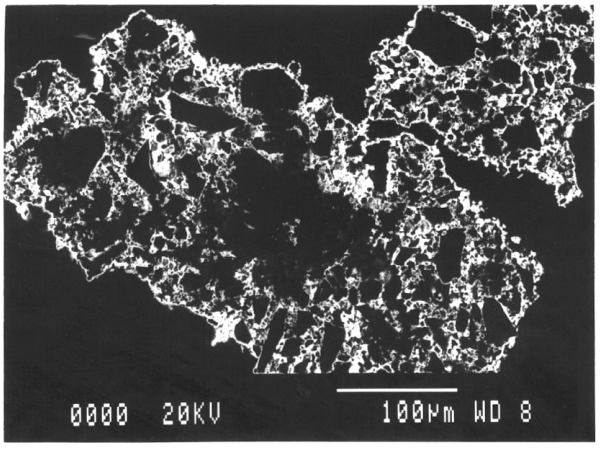

FIG. 4. SEM cross section picture of the intermediate at 7 min and 993 K.

sublimation of the oxide was responsible for the spreading (23). This was confirmed by the absence of vanadium oxides on the walls of the crucible and on the graphite felt covering the crucible, while volatile oxide of molybdenum was spread all around. In addition, if the reactants were set apart in the crucible, instead of being intimately mixed, and treated under the same conditions, no spreading occurred. The melting, and the reduction from the oxidation state +5 to the state +4 were thus faster than a significant sublimation; at 950 K the vapour pressure of V_2O_5 equals 0.52 Pa (22), which is about 100 times lower than the residual pressure of the reactor chamber. The fast release of CO corresponding to the sharp pressure peak was thus due to

$$V_2O_5 + C \rightarrow CO + 2VO_2.$$

A second broader peak of pressure was observed 10 to 20 min after the beginning of the reaction and, according to the XRD analysis (Figs. 3c and 5a) only showing the V_2O_3 pattern, was the result of a further reduction from VO_2 to V_2O_3:

$$2VO_2 + C \rightarrow CO + V_2O_3.$$

After 30 min the carbide V_8C_7 was observed by XRD analysis beside V_2O_3 (Fig. 5b). At this point the reaction slowed down (inducing less noticeable pressure variations), and several crystalline phases were simultaneously observed; it was only after 7 h of thermal treatment that XRD showed V_8C_7 alone (Fig. 5g). V_2O_3 was progressively disappearing to the benefit of $VO_{0.9}$ and traces of V_2C (Figs. 5c–f), and the last hours of reaction only consisted

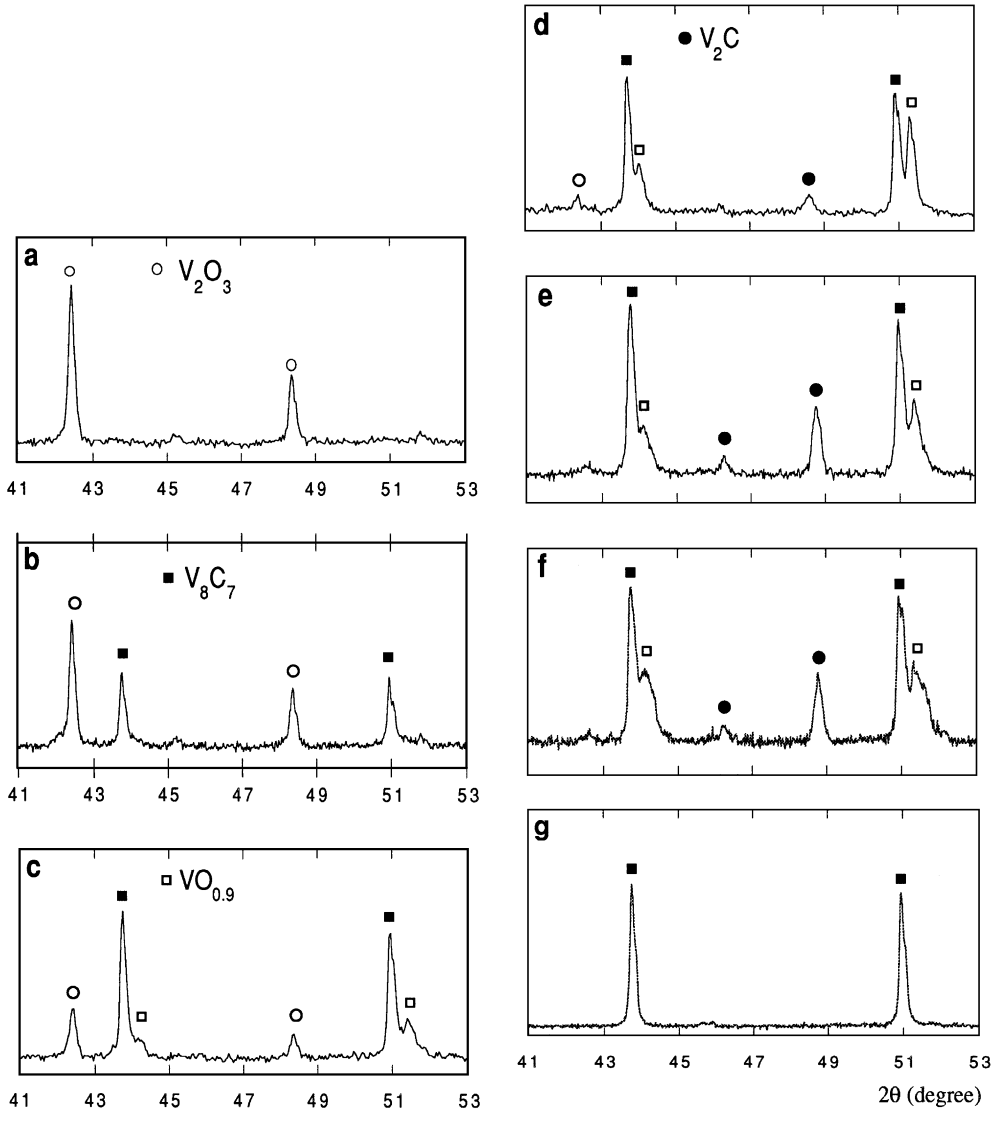

FIG. 5. XRD pattern of the intermediate at: (a) 21 min and 1393 K; (b) 30 min and 1473 K; (c) 40 min and 1526 K; (d) 60 min and 1548 K; (e) 2 h and 1563 K; (f) 4 h and 1563 K; (g) 7 h and 1563 K. JCPDS files: V_2O_3 34-187; V_8C_7 35-786; $VO_{0.9}$ 10-313; V_2C 19-1393; 24-1390. Y-scale: intensity (a.u.).

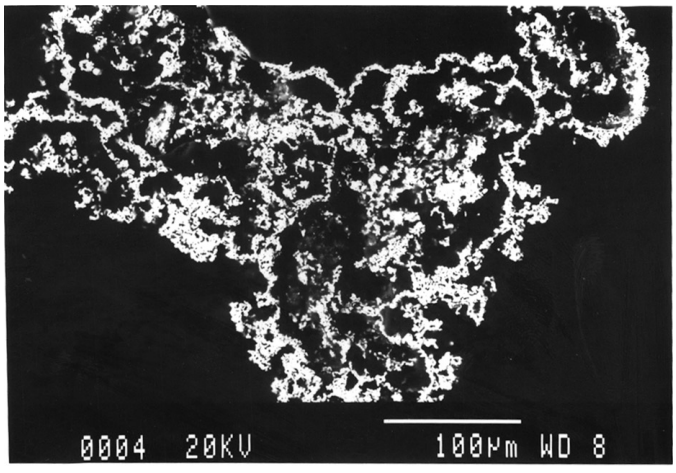

FIG. 6. SEM cross section picture of the final product after 7 h at 1563 K.

of the conversion of $VO_{0.9}$ into V_8C_7, which are isomorphous. They both exhibit a face centered cubic network of vanadium atoms, with a measured cell parameter of $4.12 \pm .02$ Å for $VO_{0.9}$ and of $4.16 \pm .02$ Å for V_8C_7. Another intermediate product was also observed by XRD with its main diffraction lines at $d = 2.28 \pm .01$ Å ($2\theta = 46.2°$) and $d = 2.17 \pm .01$ Å ($2\theta = 48.8°$). This species was not identified using X-ray diffraction by comparison with a reported structure in the literature, but it seems to be similar to the hexagonal V_2C (JCPDS 24-1390) or its orthorhombic distortion (JCPDS 19-1393); it should be emphasized that V_2C was always observed when the initial mixture was deficient in carbon which was consistent with the stoichiometry of this carbide. A cross section SEM picture of the final vanadium carbide V_8C_7 is shown in Fig. 6. The homogeneous dispersion of the vanadium observed on the precursor (Fig. 4) was maintained (the clear zone of the picture). The voids left by the carbon which had reacted could be observed; this underlines that the "shape memory" concept was valid, keeping the shape of the initial carbonaceous frame. This is also well illustrated on the SEM pictures shown in Fig. 7, where a graphitic fibre of carbon was converted into a pipe of V_8C_7. The initial carbon shape was in fact replaced by its carbidic print meaning that the second step of the reaction, the reduction of the oxide layer, proceeded through the diffusion of the internal carbon towards the surface oxide, which explained, together with the formation of CO (the thermodynamic driving force of the synthesis), the high specific surface area of the final product. The same phenomenon was observed during the synthesis of Mo_2C (23).

3.2. BET Analysis

In Fig. 8, the amount of nonreacted carbon and the specific surface area of the material are presented as a function of the reaction time (see Table 1 for numerical values). Just before the spread of VO_2 over the charcoal, the surface area of the mixture was 447 ± 10 m^2 g^{-1}, which corresponded to the only contribution of the active charcoal (457 ± 20 m^2 for the amount contained in 1 g of product), V_2O_5 having a negligible surface contribution. During the consumption of the carbon the surface decreased to about 230 m^2/g after 2 h of reaction. The following consumption of carbon did not affect the surface area; this fact emphasizes the minor effect of the remaining charcoal surface area on the specific surface of the carbide. This means that the remaining charcoal was embedded within the carbide and only played a mechanical role. It has been possible to prepare pure carbide without any residual carbon at quite high specific surface areas (about 50 m^2/g); however, the use of charcoal in excess was preferred, as it shortened the reduction and the carburization time and lowered the reaction temperature, yielding a stronger product in terms of mechanical properties.

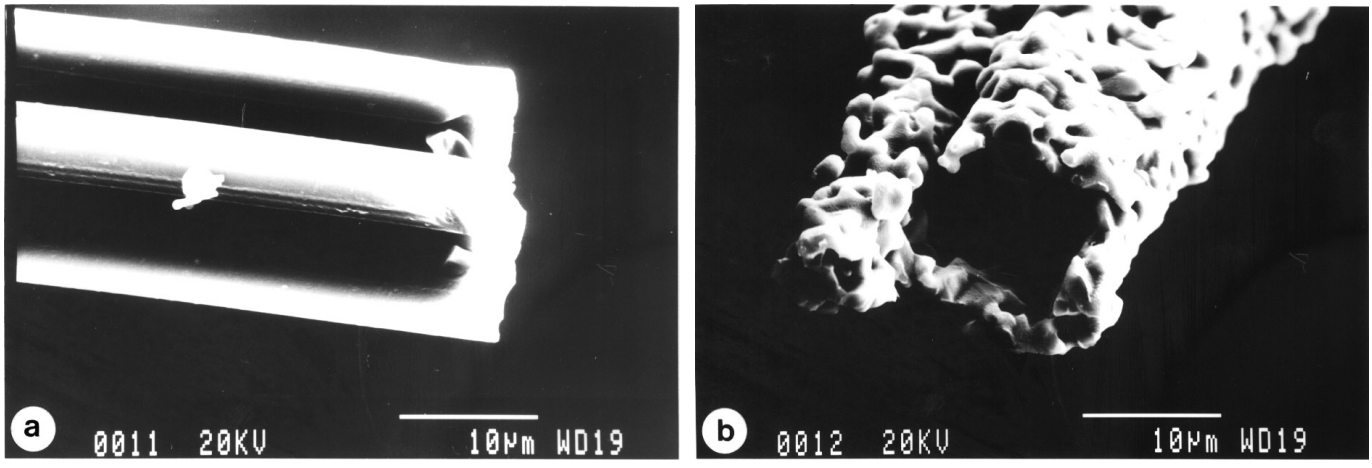

FIG. 7. Scanning-electron micrograph of a graphitic fibre before (a) and after (b) reaction (7 h at 1563 K).

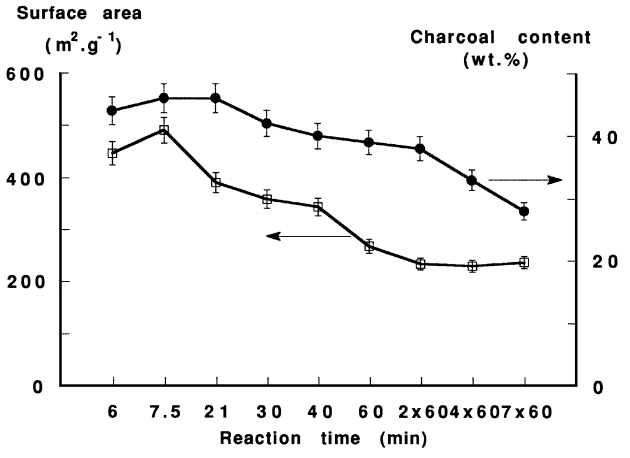

FIG. 8. Evolution of the sample surface area and its charcoal content with reaction time (nonlinear scale).

3.3. TPR and HRTEM Analyses

In Fig. 9 are shown the TPR profiles of the fresh carbide passivated by air at room temperature, of the same carbide left for 5 weeks in air and of pure V_2O_5 for comparison. No oxygen was detected on the fresh product even if the elemental analysis gave an O/V atomic ratio of 0.09, meaning that the oxygen was very strongly bond to vanadium atoms. After 5 weeks in air it was possible to detect a water peak at 340 K corresponding to the desorption of adsorbed water and a stronger one at 700 K, probably corresponding to the reduction of a layer of vanadium oxide on the carbide surface. After several months, a change of colour was noticeable; initially grey, the product changed to green and then orange like V_2O_5.

The HRTEM picture of Fig. 10 shows that the carbide surface, after synthesis and air passivation at room temperature, was completely covered by an amorphous phase 4 to 30 nm thick. The EDS analysis performed on this phase indicated the presence of V, O, and C. The bulk cristalline phase corresponded to the (222) plane of the V_8C_7 structure with the interplanar spacing $d = 2.40 \pm 0.10$ Å. The images taken at this high magnification showed that this vanadium carbide contained a high density of planar defects and dislocations. Many amorphous domains were also observed within the material.

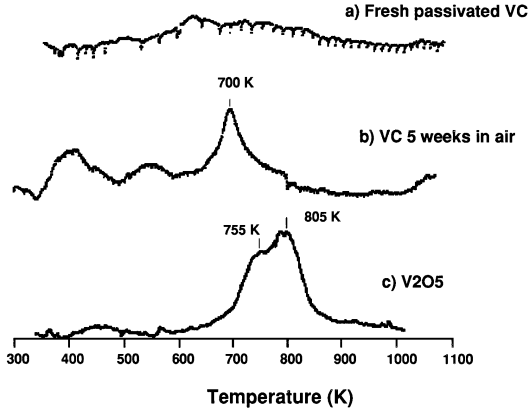

FIG. 9. TPR patterns of a vanadium carbide prepared 7 h at 1563 K: (a) Fresh and passivated (95 mg); (b) air at room temperature for 5 weeks (94 mg); (c) Strem V_2O_5 (3 mg).

3.4. NMR Analyses

The ^{51}V metal solid NMR and the ^{13}C MAS-NMR spectra are presented in Figs. 11 and 12. The ^{51}V spectrum showed the presence of a central resonance peak plus six quadrupolar peaks due to the spin 7/2 of ^{51}V. This quadrupolar splitting showed that some of the vanadium atoms were not present in a cubic symmetry as they should be in a "V_8C_8" but in different symmetries which induced electric field gradients (21, 24). The observed XRD structure was V_8C_7 and not VC or V_8C_8, the understoichiometry of the carbon induced a local loss of the cubic symmetry. A detailed analysis of the pseudo-NaCl structure of V_8C_7 containing carbon vacancies showed that a unit cell contains 32 vanadium atoms, 14 (44%) fully saturated by 8 carbon atoms and 18 (56%) bearing one carbon vacancy (i.e., surrounded by 7 carbon atoms). The addition of two simulated spectra, each of them corresponding to the 44% and the 56% V atoms, respectively, did not fit with the experimental spectrum. The addition of a third spectrum corresponding to V atoms surrounded by two carbon vacancies repelling themselves (i.e., in diagonal opposition, thus with a greater quadrupolar effect) gave an excellent fit (Fig. 11). The area of each of these three spectra should be proportional to the relative amount of each type of V atoms, V_0 with no carbon vacancies, V_1 with one, and V_2 with two vacancies. The measurement of these areas gave 72% V_2, 21% V_1, and 7% V_0. The location of the vacancies in diagonal opposition explained why so many V atoms belonged to the V_2 family. Indeed, associated pairs of neighbouring vacancies would affect far less V atoms. Such a large number of carbon vacancies could easily account for the large number of local crystalline defects observed by HRTEM or, even for the pseudo-amorphic phase also observed by microscopy.

In order to obtain more information a ^{13}C MAS-NMR was performed on the same sample. Figure 12a shows that three main peaks were found. A broad one centered at 108 ppm corresponding to the unreacted carbon (the width being due both to different electron environments and to traces of iron impurities, Fig. 12b). Two other sharp peaks at 262 and 236 ppm were attributed to two different carbon atoms in the vanadium carbide, by comparison with the carbon in Mo_2C found at 275 ppm (25). The integration of the surface of these peaks gave a ratio 2 : 1. Carbon atoms in the vanadium carbide with different electronic environments (thus, with different chemical shifts in NMR)

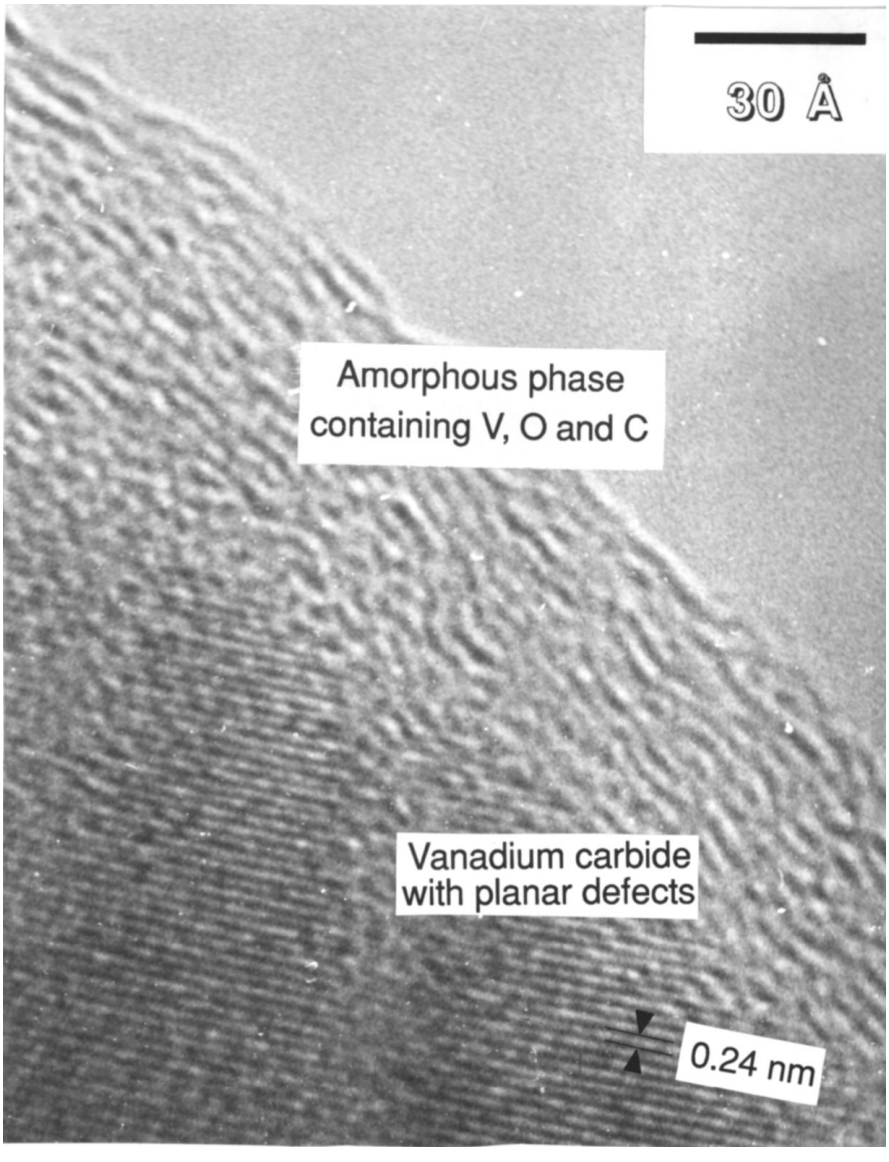

FIG. 10. HRTEM picture of the vanadium carbide (7 h at 1563 K): evidence of an amorphous layer surrounding more crystallised areas and of stacking faults in the vanadium carbide.

were expected, as these atoms were surrounded by three sorts of V atoms. If, for instance, a carbon atom was surrounded by many V_2-type vanadium atoms, its chemical shift should have been larger than the one of a carbon atom with a lower electron density—i.e., surrounded by V atoms with less carbon vacancies, V_1 and V_0, for instance. It was, however, unexpected to find only two well-resolved peaks because, intuitively, one was expecting a large family of electronic environments around the carbon atoms, statistically distributed according to the population of the three vanadium atom types and, in consequence, a broad peak or no visible peaks in the NMR spectrum. This finding means that the existence of two types of carbon atoms (or more, but with only two in a large enough quantity to be visible) could be explained either by a statistical distribution corresponding to the composition of the three types of V atoms, or by a thermodynamic condition, putting the carbon atoms in two wells of minimum energy. Unfortunately the mathematical resolution of the statistical distribution of the carbon atoms in a NaCl network containing V_0, V_1, and V_2 vanadium atoms is not trivial and we have not been able to solve it in the last 4 years; a good challenge for the readers of this article. This mathematical resolution would give an answer to the alternative between the statistics and the thermodynamics. However, it has been suggested by the ^{51}V NMR that vacancies of carbon were ordered in diagonal opposition (which meant a minimization of the energy state) and this was consistent with a thermodynamic

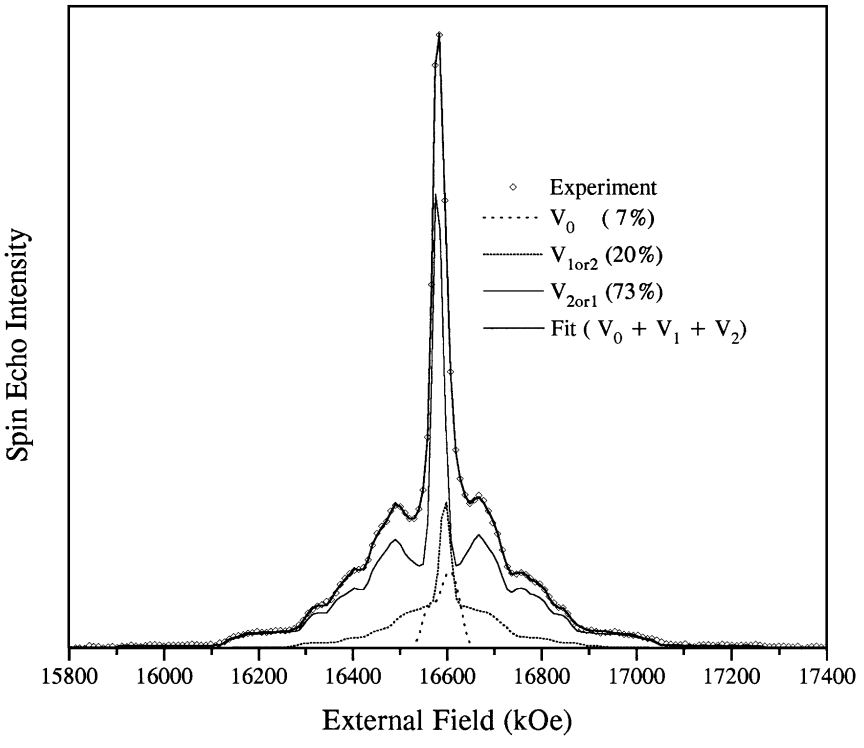

FIG. 11. ^{51}V NMR analyses of the vanadium carbide (7 h at 1563 K) and simulation.

ordering of the understoichiometric V_8C_{7-x}. The 262 ppm peak would correspond to carbon atoms having more V_2 type vanadium atoms around them than the carbon atoms corresponding to the peak at 236 ppm. The chemical analysis of the sample showed that 86.8% of the carbon atoms were contained in the nonreacted charcoal and 13.2% in the carbide, while the NMR surface integration gave 91.4% and 8.6%, respectively. The slight discrepancy could be attributed to three phenomena: experimental noise/error, a third carbide peak hidden inside the large peak of the nonreacted charcoal (less probable because this would correspond to a too-small chemical shift), or missing peaks, too small to have been detectable by NMR, corresponding to carbon atoms distributed in small quantities in different families of electronic environments.

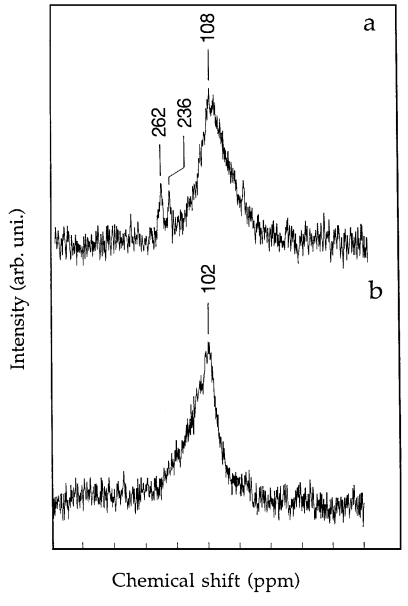

FIG. 12. ^{13}C MAS NMR analyses of the vanadium carbide (7 h at 1563 K).

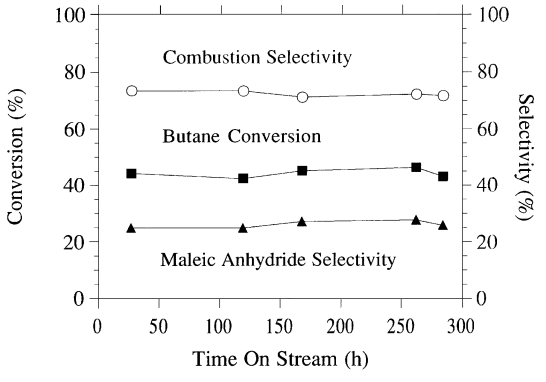

FIG. 13. Butane oxidation into maleic anhydride and combustion products. Lean mixture O_2/but = 6.

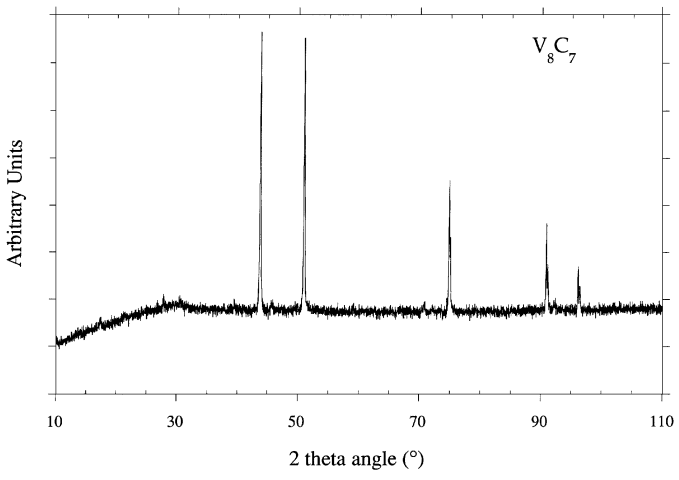

FIG. 14. XRD pattern of the catalyst before reaction.

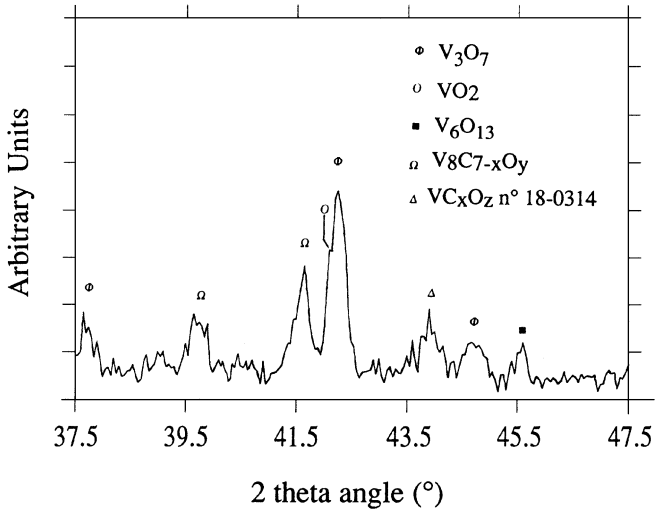

FIG. 16. XRD pattern exhibiting two "oxycarbide" phase from V_8C_7.

3.5. Catalytic Oxidation of n-Butane

V_8C_7 obtained by the synthesis described above, was tested under different reaction conditions for the *n*-butane oxidation (weight catalyst = 0.73 g, VVH = 64.7 h^{-1}, WHSV = 0.27 h^{-1}, T° = 700 K, O_2/but = 6 or VVH = 305 h^{-1}, WHSV = 1.27 h^{-1}, T° = 700 K, O_2/but = 1.1). The rich mixture, O_2/but = 1.1, gave only the combustion products CO and CO_2. The lean mixture, O_2/but = 6, produced interesting preliminary results (Fig. 13).

An accurate analysis of the XRD diagrams of the catalyst after testing under the lean mixture showed that the vanadium carbide (Fig. 14) was mainly transformed into VO_2 (in fact, V_6O_{13} and V_3O_7) and V_2O_5 (Fig. 15), plus two other solid phases in small crystalline amounts (Fig. 16), a known vanadium oxycarbide (JCPDS 18-0314), and an unknown phase (probably another oxycarbide) with its main diffraction lines appearing at 2θ angles of 39.52° and 41.61°. These two phases amounted to only 8% of the total crystalline phases, assuming that all these phases had the same sensitivity to XRD with their main peaks.

Pure VO_2 and V_2O_5 were run under similar experimental conditions and showed only very small yields for maleic anhydride formation (Fig. 17) but high activities for total combustion. It was difficult to fix the conditions in order to obtain the same conversion for all catalysts; however, for V_2O_5, VO_2, and V_8C_7 the conversions were maintained between 15 and 43% which allowed a relatively safe comparison of the selectivities. VPO was only presented for information. In consequence the relatively high yield

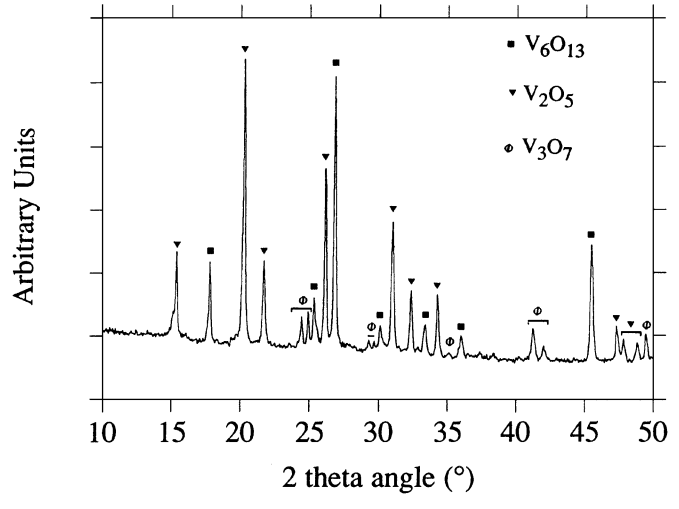

FIG. 15. XRD pattern of the catalyst after reaction.

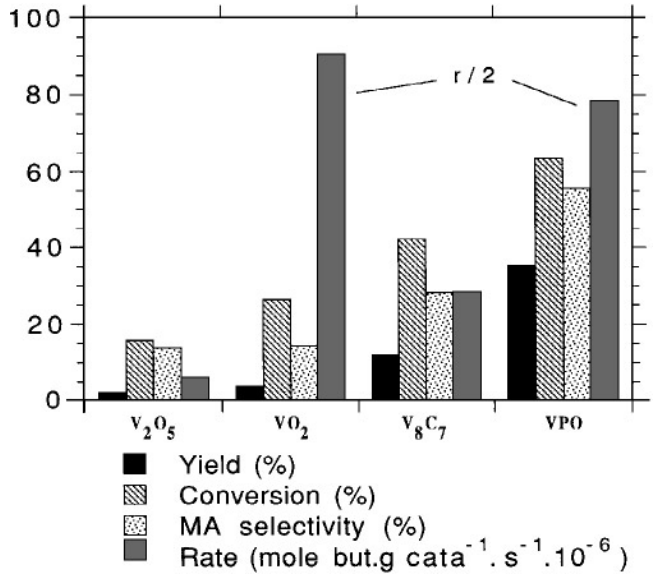

FIG. 17. Catalytic comparison between V_8C_7, V_2O_5, VO_2, and VPO for the reaction of butane to maleic anhydride.

observed on the catalyst studied was attributed to the oxycarbidic phases, the large amount of total combustion products coming from the parasite oxidic phases. Further studies to increase the amount of selective phases and to characterize their structure are currently ongoing.

4. CONCLUSION

The experiments reported above for the preparation of high surface area vanadium carbide well illustrate the principle of the shape memory synthesis applied to a meltable metal oxide precursor. From macroscopic and microscopic points of view, the spreading of the liquid V_2O_5 on the charcoal surface was clearly demonstrated by the SEM observations. The deposition occurred around the melting point of V_2O_5, and no evidence of gas phase transport was found. This spreading was favoured by the simultaneous reduction step from V_2O_5 to VO_2 ($\Delta H = +130$ kJ/mol) and by the well-known low surface tension of V_2O_5, especially with oxidic supports such as titania (27) and active charcoal surface (28). VO_2 covering the charcoal was subsequently reduced to V_2O_3, and very early some vanadium carbide V_8C_7 was observable by XRD, together with V_2O_3. The preparation of vanadium carbide by treating V_2O_5 under a H_2/CH_4 stream at 1350 K was reported to pass through V_2O_3 (4). The formation of $VO_{0.9}$ which was observed in the present study was explained by the use of a higher reaction temperature. The subsequent carburization of $VO_{0.9}$ led to the isostructural carbide V_8C_7. The V_2C-like intermediate was also formed in the course of the carburization, depending on the rate of diffusion of oxygen and carbon in the material.

The final product did not present an extra-broadening of the XRD peaks, indicating that the average size of the crystalline particles was greater than 65 nm. The theoretical BET surface area of spherical particles of this size would be lower than 8 $m^2\ g^{-1}$. As shown by the HRTEM pictures, the high surface area of the products was assigned to the amorphous phases present throughout the material. The contribution to the total surface area of the remaining charcoal was not easy to evaluate. However, the evolution of the total surface area and of the charcoal content given in Fig. 8 demonstrated the independence between them, especially the consequent decrease of carbon content after 2 h of reaction up to 7 h without variation in the total surface area. In addition the preparation of free-charcoal samples with surface areas above 30 $m^2\ g^{-1}$ supported the efficiency of the method which was much higher than those reported in the literature: 0.9 $m^2\ g^{-1}$ (28), 0.3 $m^2\ g^{-1}$ (29), 5.3 $m^2\ g^{-1}$ (4) with the exception of 50 $m^2\ g^{-1}$ (30).

The high specific surface area vanadium carbide prepared by the new "shape memory" method is suitable for catalytic applications and is currently studied for oxydation or deshydrogenation reactions in its bulk and pure form, either supported, or as starting material for the preparation of oxicarbides. Preliminary results for the oxidation of *n*-butane into maleic anhydride exhibit promising properties, probably due to the ability of the transition metal carbides to form catalytically active oxycarbides under mild oxidative conditions, properties already observed on Mo_2C (12).

ACKNOWLEDGMENTS

This work was financially supported by Pechiney (Paris) and Du Pont de Nemours (Wilmington). The ^{13}C MAS-NMR was performed at the Laboratory of Catalysis of the Université Notre-Dame de la Paix de Namur (B) and E. G. Derouane and A. Fonseca are gratefully acknowledged. M. Benhaissa and J. Guille are also acknowledged for the electron microscopy analyses.

REFERENCES

1. Boudart, M., and Levy, R., *Science* **181**, 547 (1973).
2. Lee, J. S., Oyama, S. T., and Boudart, M., *J. Catal.* **106**, 125 (1987).
3. Ranhotra, G. S., Haddix, G. W., Bell, A. T., and Reimer, J. A., *J. Catal.* **108**, 24 (1987).
4. Schlatter, J. C., Oyama, S. T., Metcalfe III, J. E., and Lamber, J. M., Jr., *Ind. Eng. Chem. Res.* **27**, 1648 (1988).
5. Ribeiro, F. H., Dalla Betta, R. A., Boudart, M., Baumgartner, J., and Iglesia, E., *J. Catal.* **130**, 86 (1991).
6. Ribeiro, F. H., Boudart, M., Dalla Betta, R. A., and Iglesia, *J. Catal.* **130**, 498 (1991).
7. Iglesia, E., Baumgartner, J., Ribeiro, F. H., and Boudart, M., *J. Catal.* **131**, 523 (1991).
8. Ledoux, M. J., Pham-Huu, C., Guille, J., and Dunlop, H., *J. Catal.* **132**, 383 (1992).
9. Ledoux, M. J., Pham-Huu, C., Guille, J., Dunlop, H., Hantzer, S., Marin, S., and Weibel, M., *Catal. Today* **15**, 263 (1992).
10. Ledoux, M. J., Guille, J., Pham-Huu, C., and Marin, S., U.S. Patent 5,139,987 (1992) and European Patent 0,474,570B1 (1995).
11. Pham-Huu, C., Ledoux, M. J., and Guille, J., *J. Catal.* **143**, 249 (1993).
12. Blekkan, E. A., Pham-Huu, C., Ledoux, M. J., and Guille, J., *Ind. Eng. Chem., Prod. Res. Dev.* **33**, 1657 (1994).
13. Ledoux, M. J., Guille, J., Pham-Huu, C., Dunlop, H., and Prin, M., European Patent 0,534,867 (1995).
14. Storms, E. K., "The Refractory Carbides," Academic Press, New York, 1967.
15. Toth, L. E., *Transition metal carbides and nitrides*, Academic Press, New York, 1971.
16. Ledoux, M. J., Hantzer, S., Guille, J., and Dubots, D., U.S. Patent 4914070 (1990) and Eupropean Patent 0313480 (1992).
17. Ledoux, M. J., Hantzer, S., Pham-Huu, C., Guille, J., and Desaneaux, M. P., *J. Catal.* **114**, 176 (1988).
18. Lee, J. S., Locatelli, S., Oyama, S. T., and Boudart, M., *J. Catal.* **125**, 157 (1990).
19. Oyama, S. T., Schlatter, J. C., Metcalfe III, J. E., and Lambert, J. M., Jr., *Ind. Eng. Chem. Res.* **27**, 1639 (1988).
20. Lee, J. S., Volpe, L., Ribeiro, F. H., and Boudart, M., *J. Catal.* **112**, 44 (1988).
21. Panissod, P., "Topics in Current Physics" (U. Gonser, Ed.), Vol. 40, p. 396, Springer-Verlag, New York/Berlin, 1986.

22. Kubaschewski, O., and Evans, E., "La thermochimie en métallurgie," p. 353, Gauthier-Villard, Paris, 1964.
23. Pham-Huu, C., Thèse de Chimie, ULP, Strasbourg, 1991.
24. Ledoux, M. J., Michaux, O., Agostini, G., and Panissod, P., *J. Catal.* **96**, 189 (1985).
25. Ledoux, M. J., Pham-Huu, C., Delporte, P., Blekkan, E. A., York, A. P. E., Derouane, E. G., and Fonseca, A., *in* "Proc. TOCAT-2," Studies in Surface Science and Catalysis (Y. Izumi, H. Arai, and M. Iwamoto, Eds.), Vo. 92, p. 81, Elsevier, Amsterdam, 1995.
26. Machej, T., Haber, J., Turek, A. M., and Wachs, I. E., *Appl. Catal.* **70**, 115 (1991).
27. Bansal, R. C., Donnet, J. B., and Stoekli, F., "Active Carbon," Dekker, New York, 1988.
28. Samsonov, G. V., Bulankova, T. G., Khodak, P. A., Prshedromirskaya, E. M., Sinel'nikova, V. S., and Sleptsov, V. M., *Kinet. Katal.* **10**, 1057 (1969).
29. Il'chenko, N. I., *Kinet. Katal.* **18**, 153 (1977).
30. Kapoor, R., and Oyama, S. T., *J. Solid State Chem.* **120**, 320 (1995).